ISSN 1068-3666, Journal of Friction and Wear, 2015, Vol. 36, No. 4, pp. 293–300. © Allerton Press, Inc., 2015.
Original Russian Text © R.I. Nepershin, 2015, published in Trenie i Iznos, 2015, Vol. 36, No. 4, pp. 384–393.

# Plastic Deformation of Rough Surface by a Sliding Tool

**R. I. Nepershin**

*Moscow State University of Technology STANKIN, Vadkovskii per. 1, Moscow, 127994 Russia*
*e-mail: nepershin_ri@rambler.ru*

Received September 16, 2014

**Abstract**—Modeling is carried out of the discrete plastic deformation of the rough surface of a metal part by a sliding rigid tool with a circular profile. This modeling is based on the theory of the plane deformation of a perfectly plastic solid taking into account the Prandtl contact friction. The number of discrete contacts and the plastic stress–strain state are determined by the periodic shape of the rough surface, as well as the radius and the vertical displacement of the tool with regard to asperity summits. The plastic smoothing mode used to reduce the surface roughness without the deformation of the core of the metal part is considered.

**Keywords**: rough surface, periodic shape, plastic smoothing, rigid tool, perfect plasticity, plane deformation, slip lines

**DOI:** 10.3103/S1068366615040108

## INTRODUCTION

A serious problem in manufacturing engineering when producing precise parts with high wear resistance and surface quality is improving performance by reducing the number of manufacturing steps and selecting reasonable production methods [1]. An efficient way to solve this problem is the plastic smoothing of rough surfaces after the removal of basic tolerance using a high-performance cutting tool and the elimination of labor-consuming additional finish steps [1, 2]. Taking into account strict requirements for the precision and roughness of surfaces, high performance is especially topical in the machining of parts made of up-to-date high-temperature chromium–nickel alloys.

A plastic smoothing tool should have high rigidity, precision, and wear resistance; its surface quality should be by an order of magnitude better than that of the part under machining. To this end, the plasma deposition of wear-resistant coatings is efficient [3].

Plastic smoothing belongs to processes of the surface plastic deformation (SPD) of metal parts aimed at improving the wear resistance and quality of their surfaces. In the majority of SPD processes, plastic deformation propagates to a depth that substantially exceeds the height of microasperities. The modeling of stationary SPD processes during the sliding and rolling of tools with various shapes is considered in works [4, 5]. These results are of interest from the viewpoint of estimating process parameters of SPD and studying problems of rolling and sliding friction under heavy loads [6].

The difference of plastic smoothing from SPD consists of a decrease in the surface roughness due to the deformation of microasperities. During the horizontal sliding of a tool, discrete contacts continuously change, the area of the contact expands, the contact pressure increases, surface valleys become filled with the material, and the surface roughness decreases.

In this work, we carry out the modeling of the process of the plastic smoothing during the sliding of a rigid tool with a circular profile over a rough surface with a periodic shape of asperities and valleys, which is determined by the machining parameters. At high plastic deformations of asperities of the surface being machined, the model of a perfectly plastic solid can be used [7–9]. The tool with the circular-shaped working surface is assumed to be rigid and to have a roughness negligibly small as compared to that of the surface being machined. The Prandtl contact friction stress is taken into account. The ultimate deformation of asperities of the original roughness of the surface under machining is limited by a high Prandtl contact pressure; when the contact pressure begins to exceeding this pressure, plastic deformation propagates deep into the surface layer following the mechanisms considered in works [4, 5].

## PROBLEM FORMULATION AND BASIC EQUATIONS

Figure 1 shows the plastic deformation of the rough surface by the rigid tool with the circular contact surface. The roughness of the tool surface is assumed to be negligibly small as compared to the roughness of the part surface, which, after machining, has the periodic shape with straight boundaries of the asperities and valleys.

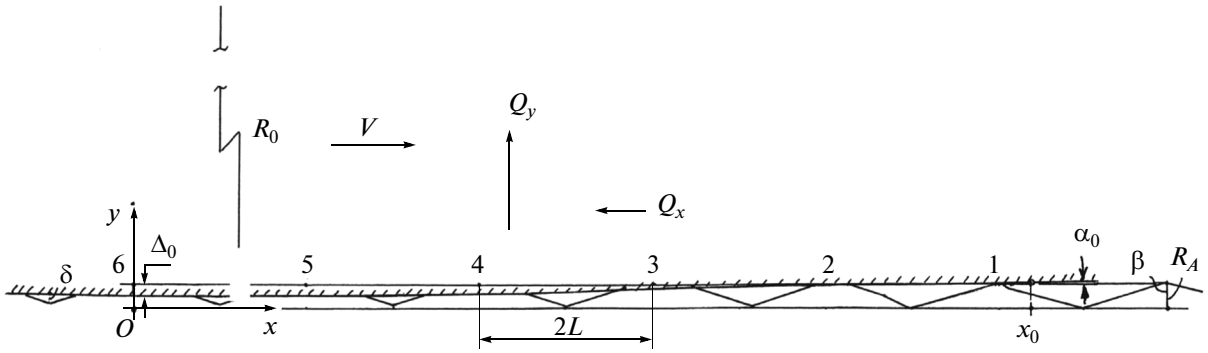


**Fig. 1.** Plastic deformation of rough surface by sliding tool. (1)–(6) are numbers of deformed asperities.

The height of asperities with regard to the line of valleys is taken to be the characteristic linear dimension $R_A = 1$. The dimensionless half-length $L$ between and the asperities and the valleys is related to the half-angle $\beta$ at asperity summits and valleys by the formula $L = \tan\beta$. The discrete plastic deformation of the asperities occurs during the horizontal sliding of the tool over the surface under machining with the velocity $V$ and the vertical displacement $\Delta_0 < 1/2$ of the lowest point of the circular profile of the tool with the radius $R_0$. The zone of discrete contacts is determined by the angle $\alpha_0$ at the intersection of the boundary of the tool with the line of valleys. Under the condition $R_0 \gg 1$, the angle $\alpha_0$ and the number of the discrete contacts $N_c$ are determined by the following formulas:

$$\alpha_0 = \sqrt{2\frac{\Delta_0}{R_0}}, \tag{1}$$

$$N_c = \mathrm{int}(R_0\alpha_0/2L) + 1. \tag{2}$$

During the sliding of the tool, the asperity that is offset by $2L(N_c - 1)$ from the origin of coordinates $O$ is first to come into contact. Plastic deformation ceases at the asperity with the number $N_c$ at $x = 0$. Under the condition $\alpha_i \ll 1$, the distances $x_i$, the angles of slope of the tangent to the profile of the tool $\alpha_i$, and the vertical deformations $\Delta_i$ of the deformed asperities with the numbers $i = 1, 2, \ldots, N_c$ are determined by the following formulas:

$$x_i = 2L(N_c - i), \quad \alpha_i = \frac{x_i}{R_0},$$
$$\Delta_i = \Delta_0 - \frac{1}{2}R_0\alpha_i^2, \quad i = 1, 2, \ldots, N_c. \tag{3}$$

Because the angles $\alpha_i$ are small, we take the shape of the boundary of the tool when the asperities with the numbers $i$ are deformed to be straight with the angles of slope to the $x$ axis $\alpha_i$ and consider the plane plastic deformation of a perfectly plastic solid [7–9].

The unit of the stress is the doubled plastic constant $2k = 1$, where $k = \sigma_s/\sqrt{3}$, taking into account high plastic deformations of the asperities. At the boundary of the tool, the Prandtl contact friction stress $\tau_c < 0.5$ is taken into account. Plastic flow obeys the following differential equations of the slip lines $\xi$ and $\eta$:

$$\frac{dy}{dx} = \tan\varphi \text{ for } \xi \text{ and } \frac{dy}{dx} = -\cot\varphi \text{ for } \eta, \tag{4}$$

where $\varphi$ is the angle of slope of the tangent to the slip line $\xi$ with the $x$ axis by the Hencky relations for the average stress $\sigma$ and the angle $\varphi$

$$\sigma - \varphi = \text{const along } \xi \text{ and } \sigma + \varphi = \text{const along } \eta, \tag{5}$$

and by the Geiringer relations for the projections of the velocities $V_\xi$ and $V_\eta$ on the slip lines

$$dV_\xi - V_\eta d\varphi = 0 \text{ along } \xi$$
$$\text{and } dV_\eta + V_\eta d\varphi = 0 \text{ along } \eta. \tag{6}$$

Equations (4) and (5) make up the system for calculating coordinates of node points of the slip lines, as well as values of $\sigma$ and $\varphi$ in these points, using numerical procedures presented in work [10]. Equations (6) determine the orthogonal reflections of the curved slip lines $\xi'$ and $\eta'$ on the plane of the hodograph of the velocities $V_x$ and $V_y$

$$dV_y/dV_x = \tan\varphi \text{ for } \eta'$$
$$\text{and } dV_y/dV_x = -\cot\varphi \text{ for } \xi', \tag{7}$$

which are used to calculate the velocity field on the hodograph plane.

During the deformation of first asperities at small displacements $\Delta_i$, the geometric similarity of the expanding plastic zone is retained. This deformation is described by the model of the asymmetric plastic deformation of a wedge by a sliding inclined tool. As the asperities continue to move toward point $O$ (Fig. 1), the vertical displacements $\Delta_i$ grow to the maximum value $\Delta_0$, the length of the discrete contacts increases, a nonstationary plastic zone is formed, and the valleys become filled with the material. The assigned value $\Delta_0$ is restricted by the limiting pressure applied to the tool, which leads to the deformation of

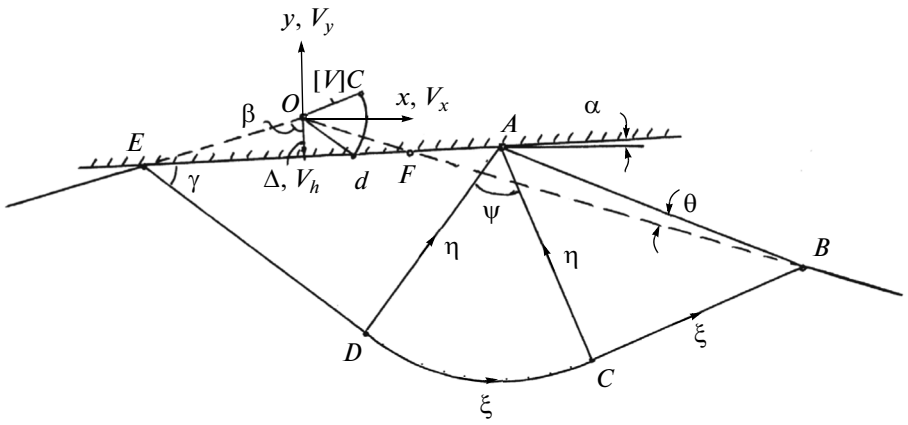


**Fig. 2.** Slip lines and velocity hodograph at first stage of deformation. Combined unit diagram.

the core of the part and the formation of a plastic zone with the depth exceeding the height of the asperity $R_A$.

## FIRST STAGE OF DEFORMATION

Figure 2 shows the slip lines and the velocity hodograph of the automodeling stage of the deformation of the asperities in the coordinates $x$, $y$ with the origin $O$ placed at the summit of an asperity in the form of the combined unit diagram. As the unit of the length, we take the vertical displacement $\Delta$ and, as the unit of the velocity, we take the vertical velocity of the embedment of the tool $V_h = V\tan\alpha$. In this unit diagram, the plastic zone and the velocity hodograph remain unchanged because of the geometric similarity of the expanding plastic zone.

During the sliding of the tool, the asymmetric deformation of the asperity occurs and the material is displaced on the inclined boundary $AB$ at the angle $\theta$ to the right boundary of the asperity. The stresses in the plastic zone $ABCDE$, which obey Eqs. (4) and (5) with the boundary condition $\sigma = -0.5$ at the free boundary $AB$ and the condition of contact friction $\tau_c = \mu$ at the boundary $AE$, are determined by the uniform stress state in the zones $ABC$ and $ADE$, as well as the centered spiral fan with the angle of the fan $\psi$ at point $A$. The normal pressure applied to the tool is found using the following formula:

$$p = \psi + 0.5(1 + \sin 2\gamma), \quad \text{where } \gamma = 0.5\arccos 2\mu. \quad (8)$$

From the equality of the areas of the triangles $OEF$ and $ABF$, as well as the condition of the plastic incompressibility, the following transcendental equation for the angle $\theta$ can be derived:

$$b[\cos\nu - \sqrt{2}\sin\gamma\sin\theta]^2 - \sin\theta\cos(\theta + \nu) = 0, \quad \nu = \alpha - \beta, \quad (9)$$

$$b = \frac{1}{4}\frac{\cos^2\alpha}{\sin^2\gamma}\frac{\left(\cot^2\beta - \tan^2\alpha\right)}{\cos\nu\cot\beta}.$$

In the small-angle approximation, the solution to Eq. (9) can be written as follows:

$$\theta = b\frac{\cos\nu}{1 + 2\sqrt{2}\sin\gamma}. \quad (10)$$

The improved value of the angle $\theta$ is found by solving Eq. (9) using the Newton method. The length of the boundary of the contact $l_c$ and the angle of the spiral fan $\psi$ are then calculated as follows:

$$l_c = a\cos\nu[\cos\nu - \sqrt{2}\sin\gamma\sin\theta]^{-1},$$
$$\nu = \alpha - \beta, \quad a = 2\cot\beta\left[(\cot^2\beta - \tan^2\alpha)\cos\alpha\right]^{-1}, \quad (11)$$

$$\psi = \beta + \gamma - (\pi/4 + \alpha + \theta). \quad (12)$$

The forces that act on the tool increase in the linear proportion with growing displacement $\Delta$ and are determined by the contact stresses as follows:

$$Q_x = l_c\Delta(p\sin\alpha + \mu\cos\alpha),$$
$$Q_y = l_c\Delta(p\cos\alpha - \mu\sin\alpha). \quad (13)$$

The plastic deformation is determined by the velocity hodograph $cd$ with the break along the rigid-plastic boundary $[V] = \cos\alpha/\sin\gamma$, which gives rise to the jump of the equivalent plastic deformation; this jump occurs when material points cross the rigid-plastic boundary. The distribution of the deformation in the zone $ACD$ can be found by the numerical integration of the trajectories of the movement of the material points in the unit diagram [7, 8].

The ultimate value of $\Delta_1^*$ at which the automodeling stage of the deformation of the asperity still persists is determined by the shift of point $B$ to the lowest point of the valley.

## SECOND STAGE OF DEFORMATION

Upon reaching the inequality $\Delta > \Delta_1^*$, the filling of the right valley and the plastic flow of the left boundary of the asperity begin. Figure 3 shows the slip lines that

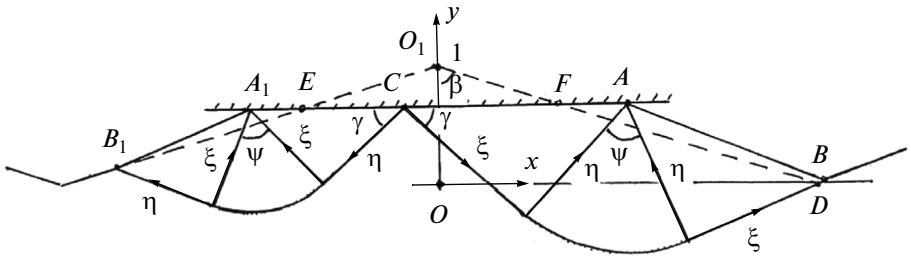


**Fig. 3.** Slip lines at second stage of deformation.

are determined by the free boundaries $AB$ and $A_1B_1$. The angle of slope of the right boundary $AB$ to the initial inclined boundary of the asperity $\theta_1 = \theta$, the angle $\psi$ of the spiral fan at point $A$, and the pressure $p$ at the interface with the tool are the same as those considered at the first stage. From the condition of the continuity of the pressure $p$ at the interface $AA_1$, there follows an equality of the angles of the spiral fan $\psi$ at points $A$ and $A_1$ in the right and left plastic zones with the angle of slope $\theta_2 = \theta_1 + 2\alpha$ of the left boundary $A_1B_1$ to the left initial boundary of the asperity.

It follows from the condition of plastic incompressibility that the area $S_0$ of the triangle $EFO_1$

$$S_0 = \Delta^2 \cot\beta/(\cot^2\beta - \tan^2\alpha) \qquad (14)$$

is equal to the sum of the area $S_1$ of the quadrangle $ABDF$ on the right face and the area $S_2$ of the triangle $A_1B_1E$ on the left face of the deformed asperity. If the coordinates of point $A$ are known, the coordinates of point $B$ can be found at the intersection of the straight lines $AB$ and $BD$. Therefore, the area $S_1$ is the function of the coordinate $x_A$ of point $A$. The area $S_2$ is determined by the coordinates of points $A_1$ and $E$, as well as point $B_1$, which lies at the intersection of the straight line $A_1B_1$ with the left inclined boundary of the asperity. The calculation of the area $S_2$ yields a quadratic equation for the coordinate $x_{A1}$ point $A_1$. Since $S_2 = S_0 - S_1(x_A)$, the coordinate $x_{A1}$ is also a function of the coordinate $x_A$.

The conjugation of the right and left plastic zones at point $C$ leads to the following transcendental equation for the coordinate $x_A$:

$$l_1(x_A) + l_2(x_A) - (x_A - x_{A1}(x_A))\sqrt{2}\sin\gamma/\cos\alpha = 0, \qquad (15)$$

where $l_1$ and $l_2$ are the lengths of the free boundaries $AB$ and $A_1B_1$ of the right and left plastic zones. At $\Delta = \Delta_1^*$, the left plastic zone is contracted to point $E$ and the coordinate $x_A$ is the same as that considered at the first stage of deformation. At the value of $\Delta > \Delta_1^*$ close to $\Delta_1^*$, the initial approximation for $x_A$ is taken to be equal to the value of $x_A$ at $\Delta = \Delta_1^*$. The solution of Eq. (15) using the Newton iteration method yields the value of $x_A$ at $\Delta > \Delta_1^*$ and the coordinate $x_{A1}$. The length of the boundary of the contact is then determined as follows: $l_c = (x_A - x_{A1})/\cos\alpha$. The contact pressure $p$, as well as the forces $Q_x$ and $Q_y$, are found using formulas (8), (12), and (13).

The velocity hodographs of the right and left plastic zones are determined by the jump of the velocity along the rigid-plastic boundaries and have the same form as the velocity hodographs considered at the first stage of deformation. The second stage of deformation ceases upon reaching the displacement $\Delta_2^*$ at which the coordinates $y$ of points $B$ and $B_1$ coincide.

## THIRD STAGE OF DEFORMATION

Upon reaching the inequality $\Delta > \Delta_2^*$, the valleys to the right and to the left of the deformed asperity become filled with the material, which leads to a decrease in the lengths of the free boundaries of the right and left plastic zones, as well as to an increase in the pressure applied to the tool. The slip lines and the distribution of the contact pressure at the third stage of the deformation of the asperity are shown in Fig. 4.

The asymmetry of plastic flow, which comes from the preceding stage, is retained. As the displacement $\Delta$ increases and the angle $\alpha$ decreases when approaching the exit of the asperity from the plastic deformation zone, this asymmetry becomes less pronounced. At point $D$, plastic flow is divided. We determine the asymmetry of plastic flow by the relation $a_c = A_1D/AD$. The displaced areas $S_1$ and $S_2$ on the right and left faces of the asperity are related as follows: $a_c = S_2/S_1$. The condition of plastic incompressibility and the use of formula (14) for the area $S_0$ lead to the following equation:

$$(1 + a_c)S_1 = \Delta^2 \cot\beta/(\cot^2\beta - \tan^2\alpha). \qquad (16)$$

The calculation of the area $S_1$ and the substitution of the obtained value into (16) yield a quadratic equation for the coordinate $x_A$ of point $A$. The calculation of the area $S_2$ and the use of the relation $S_2 = a_cS_1$ in which $S_1$ is known after the calculation of the coordinate $x_A$ lead to a quadratic equation for determining the coordinate $x_{A1}$ and the length of the boundary of the contact $l_c$.

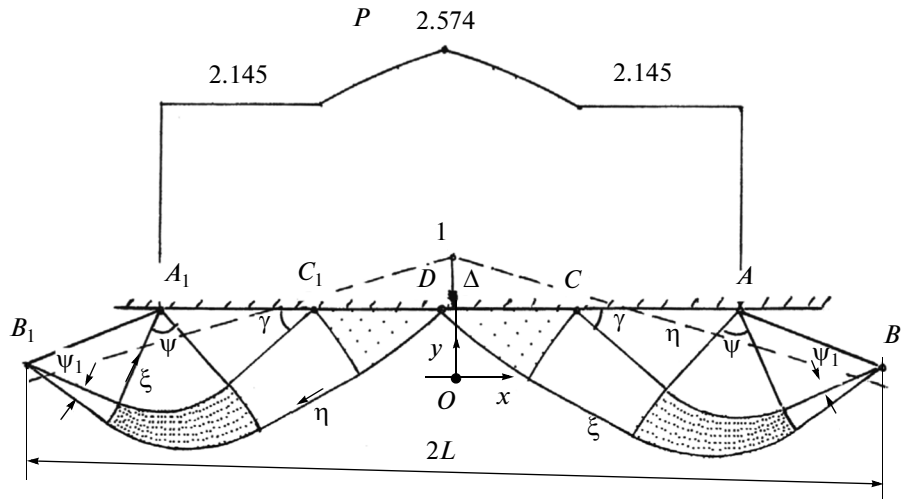


**Fig. 4.** Slip lines and contact pressure at third stage of deformation.

The slip lines in the zones $ABC$ and $A_1B_1C_1$ are determined by the lengths $l_1$ and $l_2$ of the free boundaries $AB$ and $A_1B_1$, as well as the angle of the fan $\psi$. The slip lines in the zones $BCD$ and $B_1C_1D_1$ can be found by the numerical integration of Eqs. (4) and (5) taking into account the friction at the boundaries of the contact $CD$ and $C_1D$. From the conditions of the continuity of the normal pressure at point $D$, the inequality of the angle $\psi_1$ of the centered spiral fan at points $B$ and $B_1$ follows. In the numerical solution, the length $s_1$ of the section $CD$ and the length $s_2$ of the section $C_1D$ are functions of the angle $\psi_1$, which can be found from the following equation if the length of the boundary of the contact $l_c$ is known:

$$f(\psi_1) = s_1(\psi_1) + s_2(\psi_1) + (l_1 + l_2)/(\sqrt{2}\sin\gamma) - l_c = 0. \quad (17)$$

Equation (17) is determined by calculating the slip lines, as well as the functions $s_1(\psi_1)$ and $s_2(\psi_1)$, at a stepwise increase in the angle $\psi_1$ with a small step. The range of the angles $(\psi_1)_i$ and $(\psi_1)_{i+1}$ in which the function $f(\psi_1)$ changes its sign is found. The value of the angle $\psi_1$ within this range can be found using linear interpolation.

Figure 5 presents the velocity hodograph on the plane $V_x$, $V_y$, which is determined by the jump of the velocity $[V] = \sin\alpha/\sin\gamma$ at point $D$ (Fig. 4) at the vertical velocity of the tool $V_h = \tan\alpha$. The rigid-plastic boundaries are shown in the hodograph by the arcs of circles with the angles of the centered fans $\psi$ and $\psi_1$. The plastic zones are represented in the hodograph by the curves $\xi'$ and $\eta'$ orthogonal to the slip lines, which have been found during the numerical solution of Eqs. (7). At small angles $\alpha$, the slip lines and the velocity hodographs of the right and left plastic zones become symmetric.

## FINAL STAGE OF DEFORMATION

At the final stage of the deformation of the asperity, when $\alpha = 0$ in the lowest point of the tool profile and the displacement $\Delta_0$ has the maximum value, the contact pressure applied to the instrument has also the maximum value, but no increase in the plastic deformation of the material occurs, since the vertical velocity of the sliding tool is equal to zero. The value $\Delta_0 < 1/2$ determines the final filling of the valleys between the asperities with the residual depth $\delta$ with regard to the boundary of the contact with the tool (Fig. 6). From the condition of symmetry at $\alpha = 0$ and the condition of plastic incompressibility, the following relations can be derived:

$$\Delta_0 = \frac{1}{2}[1 - \delta^2\tan(\beta - \theta)/\tan\beta], \quad (18)$$

$$\delta = l\cos(\beta - \theta), \quad (19)$$

$$l_c = 2[L - l\sin(\beta - \theta)], \quad (20)$$

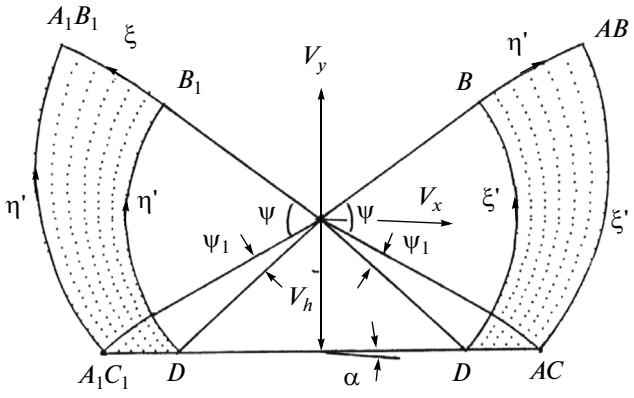


**Fig. 5.** Velocity hodograph of plastic zone shown in Fig. 4.

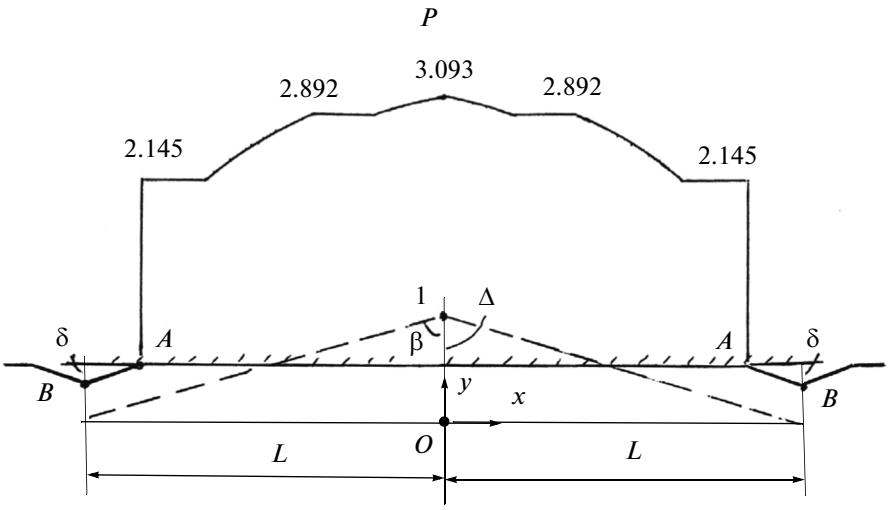


**Fig. 6.** Boundary of contact and contact pressure at final stage of deformation.

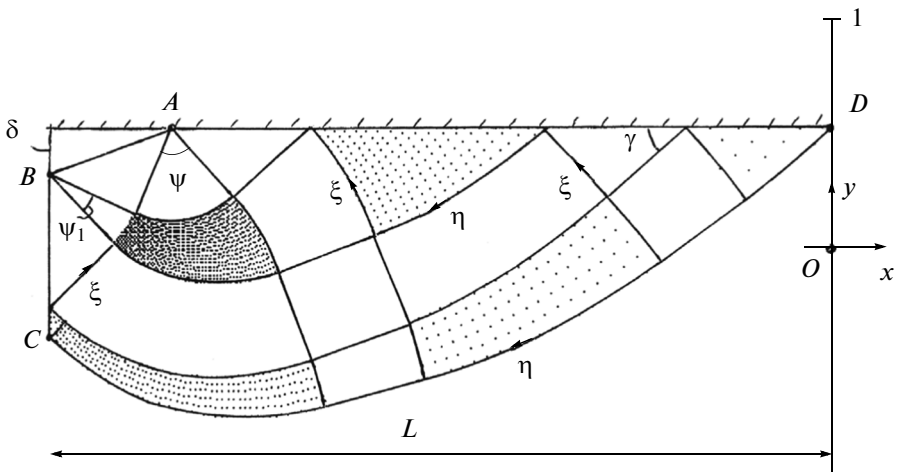


**Fig. 7.** Slip lines at final stage of deformation shown in Fig. 6.

where $l$ and $\theta$ are the length of the free boundary $AB$ and the angle of slope of this boundary to the initial lateral boundary of the asperity shown in Fig. 6 by the dashed lines.

Figure 7 shows the slip lines for the left half of the symmetric plastic zone, which depends on $\Delta_0$ and $\delta$. The angle $\psi$ of the centered spiral fan at point $A$ is determined by formula (12) at $\alpha = 0$. Upon reaching the ultimate value $\psi_1 = \pi/2 + \theta - \beta$ of the angle $\psi_1$ of the centered spiral fan at point $B$, the plastic zone propagates deep into the material along the symmetry lines $x = \pm L$. The distribution of the pressure $p$ at the boundary of the contact is determined by the values of $\sigma$ at the node points at the boundary of the contact with account for friction $\mu$ as follows:

$$p = -\sigma + 0.5\sin 2\gamma, \text{ where } \gamma = 0.5\arccos 2\mu. \quad (21)$$

## NUMERICAL MODELING

The numerical modeling of the plastic deformation of the rough surface by a circular tool was carried out using the software package in FORTRAN language to calculate the entire process and the separate stages of the deformation of microasperities.

Figure 1 shows the deformation of the rough surface with the parameters $R_A = 15$ μm, $2L = 100$ μm, and $\Delta_0 = 6.72$ μm by the tool with the radius $R_0 = 20$ mm at $\mu = 0.05$. The point of the intersection of the tool contour with the line of asperity summits is determined by the angle $\alpha_0 = 0.026$ and the coordinate $x_0 = 518.4$ μm in the deformation of six asperities. The deformation of the first and second asperities follows the model for the first stage of deformation. For the third, fourth, and fifth asperities, the asymmetric plastic flow occurs following the model for the third stage of deformation, which transits to symmetric plastic

**Table 1.** Plastic smoothing of rough surface at $R_A = 15$ μm, $2L = 100$ μm, $\Delta_0 = 6.72$ μm, $R_0 = 20$ mm, and $\mu = 0.05$

| Asperity no. | α | Δ | $l_c$ | $q$ | $Q_x$ | $Q_y$ |
|---|---|---|---|---|---|---|
| 1 | 0.025 | 0.031 | 0.276 | 2.124 | 0.028 | 0.585 |
| 2 | 0.020 | 0.181 | 1.596 | 2.124 | 0.148 | 3.400 |
| 3 | 0.015 | 0.298 | 2.628 | 2.135 | 0.215 | 5.608 |
| 4 | 0.010 | 0.381 | 3.487 | 2.150 | 0.275 | 8.269 |
| 5 | 0.005 | 0.431 | 4.504 | 2.249 | 0.276 | 10.13 |
| 6 | 0.000 | 0.448 | 4.770 | 2.323 | 0.239 | 11.08 |
| $\Sigma Q_x = 1.181$, $\Sigma Q_y = 39.07$ | | | | | | |

flow during the deformation of the sixth asperity, when $x = 0$ and $\alpha = 0$. The final depth of the valley δ at the exit from the plastic deformation zone is equal to 5.47 μm.

Table 1 presents the angles of slope of the surface of contact α, as well as the dimensionless values of the vertical displacement Δ, the length of the contact $l_c$, the average pressure $q$, and the forces that act on discrete contacts of the tool with the asperities on the rough surface. The total dimensionless values of the horizontal and vertical forces applied to the tool are equal to 1.181 and 39.07, respectively.

Figures 2 and 3 show the slip lines for the first and second stages of the deformation of the asperities on the rough surface plotted for the parameters presented in Fig. 1. Figures 4 and 5 show the slip lines with the distribution of the contact pressure and the velocity hodograph for the third stage of the deformation of the fifth asperity presented in Fig. 1.

Figures 6 and 7 shows the distribution of the contact pressure and the slip lines for the final stage of deformation, which have been calculated for the parameters of the deformation of the rough surface presented in Fig. 1 at $\Delta_0 = 0.484$. In this case, the length of the contact and the average pressure decrease to $l_c = 5.623$ and $q = 2.639$ with decreasing δ to the value of 0.2045 (3.067 μm) as compared to the case when $\Delta_0 = 0.448$ in Fig. 1. Table 2 presents the changes in the values of $q$ and δ with increasing $\Delta_0$ at the final stage of deformation for the parameters presented in Table 1.

At $\Delta_0 \to 1/2$ and $\delta \to 0$, the contact pressure $q$ rapidly increases. At the pressure $q = 1 + \pi/2$, which is equal to the pressure applied to a smooth Prandtl punch, the plastic deformation propagates to a depth of the order of the length of the contact and substantially exceeds the height $R_A$ of the asperities on the rough surface. In this case, the plastic deformation of the surface layer can be calculated without taking into account the effect of the surface roughness [8–13].

The value of the pressure $q = 1 + \pi/2$ can be considered as the ultimate value for the presented model of the deformation of the rough surface by the sliding tool. The calculation dependences of $q$ on $\Delta_0$ and δ can be used to select the process parameters when a finite value of δ is assigned.

**Table 2.** Final stage of deformation for parameters presented in Table 1 with increasing $\Delta_0$

| $\Delta_0$ | $q$ | δ |
|---|---|---|
| 0.4757 | 2.536 | 0.2519 |
| 0.4793 | 2.574 | 0.2324 |
| 0.4826 | 2.616 | 0.2134 |
| 0.4853 | 2.662 | 0.1960 |
| 0.4876 | 2.710 | 0.1801 |
| 0.4895 | 2.761 | 0.1656 |
| 0.4911 | 2.813 | 0.1524 |
| 0.4925 | 2.866 | 0.1403 |
| 0.4936 | 2.921 | 0.1293 |
| 0.4954 | 3.035 | 0.1099 |

## CONCLUSIONS

The modeling of the plastic deformation of the rough surface with the periodic shape of microasperities by the sliding tool with the circular profile describes the nonstationary processes of plastic deformation, which are accompanied by transformations of discrete contacts of the surface with the tool, as well as changes in the plastic deformation and pressure. The modeling of the entire process and its separate stages is implemented based on the theory of the plane deformation of a perfectly plastic solid using the software package in FORTRAN language.

If the vertical displacement of the tool is less than the half-height of a microasperity, the plastic deformation of the material at the exit from the zone of contact propagates to a depth of the order of the height of the asperity. The heaviest pressure arises in the contact of the asperity with the tool in the vicinity of the lowest point of the tool. With an increase in the contact pressure, the residual depth of the valleys between the deformed asperities decreases.

The ultimate vertical displacement of the tool and the minimum residual depth of the valley at the exit from the zone of contact are limited by the pressure applied to the plane Prandtl punch at which the plastic deformation propagates to a depth that substantially exceeds the initial height of the asperity.

The developed software makes it possible to carry out an analysis of the contact loads applied to the tool and the plastic deformations of the surface layer, which propagate to a depth of the order of the initial height of the surface asperity, depending on the assigned final depth of the valley between the deformed asperities.

## ACKNOWLEDGMENTS

This work was supported by the Ministry of Education and Science of the Russian Federation (project no. 9.2445.2014/K).

## NOTATION

$R_0$—radius of tool; $R_A$—height of microasperity, unit of length; $2L$—peak and valley spacing; $\beta$—half-angle at summit of asperity; $V$—horizontal velocity of sliding of tool, unit of velocity; $\alpha$—angle of slope of tangent to profile of tool in contact with deformed asperity; $\theta$—angle of slope of plastic bulge to face of asperity; $x$ and $y$—Cartesian coordinates; $\xi$ and $\eta$—slip lines; $2\sigma_s/\sqrt{3}$—Mises flow stress, unit of stress; $\mu$—dimensionless Prandtl contact friction stress; $\sigma$—average stress; $p$—normal contact pressure; $\varphi$—angle of slope of tangent to slip line $\xi$ with regard to $x$ axis; $\psi$—angle of centered spiral fan at node points; $V_\xi$ and $V_\eta$—projections of velocity on slip lines; $q$—average pressure at boundaries of contact; $Q_x$ and $Q_y$—horizontal and vertical forces per unit of length that which act on the tool; $S_0$, $S_1$, and $S_2$—areas shifted during plastic deformation of asperities; $l$, $l_1$, and $l_2$—lengths of free boundaries of plastic zone in deformation of asperities; $l_c$—length of boundary of contact of asperity with tool; $s_1$ and $s_2$—lengths of boundaries of contact of right and left plastic zones at sites with variable contact pressure; and $N_c$—number of deformed asperities at boundary of contact with tool.

## REFERENCES

1. *Mashinostroenie. Entsiklopediya. T. III-3. Tekhnologiya izgotovleniya detalei mashin* (Mechanical Engineering. Encyclopedia. Vol. III-3. Technology of Machine Detail Production), Moscow: Mashinostroenie, 2006.
2. Odintsov, L.G., *Uprochnenie i otdelka detalei poverkhnostnym plasticheskim deformirovaniem. Spravochnik* (Hardening and Finishing of Details by Surface Plastic Deformation. A Handbook), Moscow: Mashinostroenie, 1987.
3. Grigorev, S.N., Kovalev, O.B., Kuzmin, V.I., Mikhal'chenko, A.A., Fomin, V.M., Rudenskaya, N.A., and Sokolova, N.G., New possibilities of plasma spraying of wear-resistant coatings, *J. Friction Wear,* 2013, vol. 34, pp. 161–165.
4. Nepershin, R.I., On rolling and sliding of a cylinder along a perfectly plastic half-space with allowance for contact friction, *Dokl.-Phys.*, 2002, vol. 47, pp. 256–258.
5. Nepershin, R.I., Cylinder rolling and sliding on the boundary of the rigid-plastic half-space, *Prikl. Math. Mekh.,* 2003, vol. 67, pp. 326–335.
6. Drozdov, Yu.N., Yudin, E.G., and Belov, A.I., *Prikladnaya tribologiya (trenie, iznos, smazka)* (Applied Tribology (Friction, Wear, Lubrication), Moscow: Eko, 2010.
7. Hill, R., *The Mathematical Theory of Plasticity,* Oxford: Oxford Univ., 1985.
8. Sokolovskii, V.V., *Teoriya plastichnosti* (Teory of Plasticity), Moscow: Vysshaya Shkola, 1969.
9. Ishlinskii, A.Yu. and Ivlev, D.D., *Matematicheskaya teoriya plastichnosti* (Mathematical Theory of Plasticity), Moscow: Fizmatlit, 2001.
10. Druyanov, B.A. and Nepershin, R.I., *Problems of Technological Plasticity,* Amsterdam: Elsevier, 1994.

*Translated by D. Tkachuk*